Fluid Mixtures in Narrow Cylindrical Pores: Computer Simulation and Theory[1]

G. S. Heffelfinger,[2] Z. Tan,[2] K. E. Gubbins,[2] U. Marini Bettolo Marconi,[2,3] and F. van Swol[2,4]

We discuss the simulation results of phase separation of a binary Lennard–Jones mixture in a cylindrical pore induced by a temperature quench. The liquid–vapor phase separation proceeds in two stages involving different time scales. First, following the growth of density fluctuations, mechanical equilibrium is rapidly established when the system splits into a dense and a dilute phase. Material equilibrium, however, is reached via the mutual diffusion of the two components and this proceeds on an appreciably longer time scale. We briefly address the rounding of a first-order phase transition in a cylinder. In particular, we explore the possibility of multiple domains of gas and liquid when the aspect ratio is very large. Finally, we introduce an extension of Tarazona's nonlocal density function to binary mixtures of arbitrary size. The new theory is successfully tested against simulations of an additive hard-sphere mixture against a hard wall.

KEY WORDS: computer simulations; Lennard–Jones potential; mixtures (fluid); phase separation; porous media; vapor–liquid equilibrium.

1. INTRODUCTION

In recent years a number of papers have appeared that discuss fluid behavior in narrow pores. These studies are of great practical interest for enhanced oil recovery, catalysis, and gas separation and gas storage.

A variety of specific topics has been addressed, including transport phenomena (e.g., Refs. 1 and 2), capillary condensation (e.g., Refs. 3 and 4), layering transitions [5], and hysteresis [6]. Mean field density functional theory (DFT) combined with simulation has arguably been the most successful approach in elucidating the complex phase behavior of fluids in pores. Naturally, the initial emphasis has been on providing a microscopic picture for the pure fluids, and as a result we now have a successful nonlocal DFT that gives a realistic description of both phase diagrams and fluid structure and is also in close agreement with the simulations [4]. More recently, we have reported results for an example of a simple binary mixture [7]. In particular, we compared simulation results for capillary condensation with the predictions of local DFT, focusing on phase diagrams and density profiles. The latter mixture simulations simply located the liquid–vapor transition by setting up two-phase coexistence inside the pore. A nonlocal DFT for the special case of an equal-sized binary mixture has also been presented by two of us [8]. A comparision of some preliminary results of this version with a direct simulation of the same model appeared in Ref. 7. In this paper we describe how a two-phase system for a binary mixture can be produced spontaneously by performing a temperature quench during a molecular dynamics (MD) simulation. We pay special attention to the development of mechanical and material equilibrium during the quench process and we discuss the consequences of cylindrical geometry on phase separation. In addition, we introduce a generalization of Tarazona's [9] nonlocal DFT to mixtures of arbitrary size ratio and present some preliminary results for a mixture of hard spheres [10]. The theoretical predictions are tested against Monte Carlo (MC) simulations for a binary hard-sphere mixture of size ratio 1.5 against a hard wall.

2. SIMULATION METHODS

The MD method used in this paper is well documented in a number of previous publications dealing with fluid behavior in narrow pores [4, 7, 11]. Briefly, our method employs periodic boundary conditions in the z direction (along the pore axis) and temperature scaling with the equations of motion solved via a modification of Verlet's leap frog algorithm [12]. The fluid–fluid interactions between a particle of species i and a particle of species j are defined via the cut and shifted Lennard–Jones (LJ) potential,

$$\phi_{ij}(r) = \begin{cases} \phi_{ij}^{\mathrm{LJ}}(r) - \phi_{ij}^{\mathrm{LJ}}(r_{ij}^{\mathrm{c}}), & r < r_{ij}^{\mathrm{c}} \\ 0, & r \geqslant r_{ij}^{\mathrm{c}} \end{cases} \tag{1}$$

where ϕ_{ij}^{LJ} is the *full* LJ potential,

$$\phi_{ij}^{LJ}(r) = 4\varepsilon_{ij}\left[\left(\frac{\sigma_{ij}}{r}\right)^{12} - \left(\frac{\sigma_{ij}}{r}\right)^{6}\right]\tag{2}$$

with r the interparticle distance, σ_{ij} the point at which the potential is zero, and ε_{ij} the well depth. The cutoff distance used is $r_{ij}^{c} = 2.5\sigma_{ij}$; $i, j = 1, 2$. The cross parameters for the mixture are calculated according to the Lorentz–Berthelot mixing rules,

$$\sigma_{ij} = (\sigma_i + \sigma_j)/2, \qquad \varepsilon_{ij} = \sqrt{\varepsilon_i \varepsilon_j}; \qquad i, j = 1, 2, 3\tag{3}$$

These LJ parameters were taken to represent an argon (1)–krypton (2) mixture in a carbon dioxide (3) pore [7, 13],

$$\begin{array}{ll}\sigma_2/\sigma_1 = 1.066, & \sigma_3/\sigma_1 = 1.1880 \\[6pt] \varepsilon_2/\varepsilon_1 = 1.3614, & \varepsilon_3/\varepsilon_1 = 1.6307\end{array}\tag{4}$$

The fluid in the pore interacts with the solid via a one-body external field, which was taken as an average over the uniformly distributed molecules in the solid of density $\rho_3\sigma_1^3 = 0.7546$. Details of this calculation can be found elsewhere [7, 13]. No cutoff was applied to the wall–fluid interactions.

By dividing the pore into bins, both radially and axially, of size $0.1\sigma_1$ (radial) and $0.12\sigma_1$ (axial) and averaging the number of particles of component i in each bin, the *full* density profile $\rho_i(r, z)$ was obtained. By radially averaging $\rho_i(r, z)$ one obtains the *axial* density profile [7], $\rho_i(z)$, which allows the detection of a phase separation during the quench process. In a similar fashion, the chemical potential $\mu_i(r, z)$ was determined by inserting test particles of species i uniformly and randomly in the cylinder and calculating μ_i in the bins via the potential distribution theorem [8, 9]. The temperature quech was performed by instantaneously dropping the temperature from a supercritical value of $kT/\varepsilon_1 = 1.35$ to a subcritical value of $kT/\varepsilon_1 = 0.70$, where k denotes Boltzmann's constant.

To test the density functional method for arbitrary binary mixtures, which we describe in the next section, we have performed NVT–MC simulations for a binary mixture of additive hard spheres against a hard wall. A starting configuration for these simulations was obtained by arranging the spheres of both components on FCC lattice sites and choosing the density sufficiently low such that no overlaps occurred. To arrive at a dense fluid state we simply specified a high pressure p and ran a NpT–MC simulation for a box with periodic boundary conditions in all directions [16]. The periodic boundary conditions in the z direction were subsequently replaced by two hard walls and the system was then equilibrated

for at least 400,000 moves. To visualize the way in which the hard wall interacts with each type of sphere, one could imagine the wall to act on the edge of a sphere rather than on the center. Thus, if the wall is located at $z = 0$, then the center of a sphere is not allowed to have a z coordinate less than $d_i/2$. Averages for the density profiles were accumulated over 2.0×10^6 configurations using a bin width of $0.02d_1$, where d_1 denotes the diameter of the smaller sphere.

3. NONLOCAL DENSITY FUNCTIONAL THEORY

In this section we briefly outline a generalization of Tarazona's non-local density functional theory to a binary mixture of spheres with an arbitrary size ratio. The special binary mixture of equal-sized spherical molecules, for which the free energy functional of the reference fluid is just that of a *pure* hard-sphere fluid, is discussed in two other publications [7, 8]. For clarity, we restrict outselves to that part of the free energy functional that is relevant to a binary mixture of different-sized spherical molecules and hence we do not include the attractive contributions to the grand potential functional. The latter contributions can be found elsewhere (e.g., Refs. 7 and 13). The grand potential functional is given by

$$\Omega[\rho_1, \rho_2] = F[\rho_1, \rho_2] - \sum_{i=1}^{2} \int d\mathbf{r} \rho_i(\mathbf{r})[\mu_i - V_i(\mathbf{r})] \tag{5}$$

where $\rho_i \equiv \rho_i(\mathbf{r})$ and μ_i are the number density at $\mathbf{r}$ and chemical potential of species i, respectively. $V_i(\mathbf{r})$ is a one-body external field acting on a particle of species i located at $\mathbf{r}$. $F[\rho_1, \rho_2]$ is the free energy functional of a *nonuniform* hard-sphere mixture, which we calculate in the smoothed density approximation (SDA) [9, 10]. Thus, we split $F[\rho_1, \rho_2]$ into an ideal gas and a configurational contribution. The ideal-gas contribution is given exactly in terms of the local densities and the configurational (or excess) contribution is written as a function of the smoothed densities $\bar{\rho}_i$. The latter is approximated by the free energy of a *uniform* hard-sphere mixture at the smoothed densities $\bar{\rho}_i$. Thus we have

$$F^{\mathrm{id}}[\rho_1, \rho_2] = kT \sum_{i=1}^{2} \int d\mathbf{r} \rho_i(\mathbf{r})[\ln(\rho_i \Lambda_i^3) - 1] \tag{6}$$

$$F^{\mathrm{ex}}[\rho_1, \rho_2] = \sum_{i=1}^{2} \int d\mathbf{r} \rho_i(\mathbf{r}) \, \psi_i^{\mathrm{ex}}(\bar{\rho}_1, \bar{\rho}_2; \mathbf{r}) \tag{7}$$

$$\psi_i^{\mathrm{ex}}(\bar{\rho}_1, \bar{\rho}_2) = \mu_i - kT \ln(\rho_i \Lambda_i^3) - \frac{p(\bar{\rho}_1, \bar{\rho}_2)}{\bar{\rho}_1 + \bar{\rho}_2} + kT, \qquad i = 1, 2 \tag{8}$$

Here Λ_i and ψ_i^{ex} denote the de Broglie wavelength and the configurational free energy per particle of species i, respectively. The smoothed density, $\bar{\rho}_i$, is calculated as a weighted average over the density profile,

$$\bar{\rho}_i(\mathbf{r}) = \int d\mathbf{r}' W_i(\mathbf{r}, \mathbf{r}'; \bar{\rho}_1, \bar{\rho}_2) \rho_i(\mathbf{r}'), \qquad i = 1, 2 \tag{9}$$

The density-dependent normalized weighting functions W_i for species i are expanded in the smoothed densities $\bar{\rho}_1$ and $\bar{\rho}_2$. For the pure fluid Tarazona has taken this expansion to second order in the density. However, for convenience we truncate the equivalent expansion for the mixture at first order,

$$W_i(|\mathbf{r} - \mathbf{r}'|) = w_{i0}(|\mathbf{r} - \mathbf{r}'|) + \sum_{j=1}^{2} \bar{\rho}_j(\mathbf{r}) w_{ij}(|\mathbf{r} - \mathbf{r}'|), \qquad i = 1, 2 \tag{10}$$

The coefficients w_{ij} satisfy the normalization conditions

$$\int d\mathbf{r} \, w_{ij}(|\mathbf{r} - \mathbf{r}'|) = \delta_{j0}, \qquad \text{for } i = 1, 2 \quad \text{and} \quad j = 0, 1, 2 \tag{11}$$

These coefficients were determined essentially by comparing the second functional derivative of F^{ex} with respect to the density ρ_i term by term with the density expansion of the direct correlation function for the uniform hard-sphere mixture, as obtained from the Percus–Yevick (PY) approximation. The PY-compressibility equation of state was used to calculate the excess free energies. A full discussion of the details of this calculation will be published elsewhere [10]. Finally, we note that if we choose $W_i(\mathbf{r}) = \delta(\mathbf{r})$, we recover the familiar local density approximation (see, e.g., Ref. 13).

4. RESULTS AND DISCUSSION

4.1. Temperature Quench

Previously, we have presented a temperature quench for a pure fluid [11]. In particular, we have described the spontaneous phase separation of a fluid initially at a supercritical temperature when quenched into the confined fluid's two-phase region. This phase separation is manifested by gas-like and liquid-like regions separated by a hemispherical meniscus. Here we discuss the results of a temperature quench for a binary mixture. This fluid mixture was composed of $N = 780$ molecules, half of which were argon, and

the other half krypton. Initially the system was equilibrated for well over 50,000 time steps $[\Delta t = 0.005 \, (m\sigma_1^2/\varepsilon_1)^{1/2}]$ at a supercritical temperature of $kT/\varepsilon_1 = 1.35$. Subsequently we instantaneously fixed the temperature at $kT/\varepsilon_1 = 0.70$, following the system in time for 80,000 time steps. A movie of this process was produced by storing every 15th configuration and graphically reproducing it on a Silicon Graphics IRIS work station. We discuss these results aided primarily by axial density profiles. In Fig. 1 we show axial density profiles at different times during the quench process. Figure 1a contains the profile for the supercritical fluid, at reduced time, $t^* \equiv t(\varepsilon_1/m\sigma_1^2)^{1/2} = 0$, indicating uniform density and mole fraction along the pore axis. In Fig. 1b we show the axial density profile for the quenched fluid, at a temperature $kT/\varepsilon_1 = 0.70$ and time $t^* = 100$. One can see from this figure that the density is now clearly no longer uniform. Rather, a liquid phase and a gas phase which are in mechanical equilibrium coexist in the pore. Up to this point, the fluid mixture behavior is similar to that of the pure fluid. Note that the density profiles of the two components are
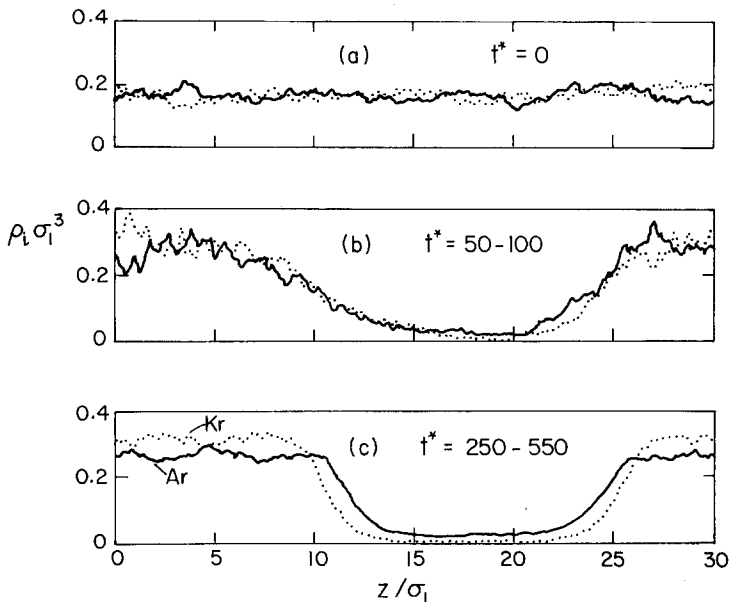
Fig. 1. Axial density profiles, $\rho_i(z)$, for a Lennard–Jones binary mixture modeled on argon (1)–krypton (2) in a cylindrical pore of carbon dioxide (3) of radius $R = 5\sigma_1$. The supercritical system, $kT/\varepsilon_1 = 1.35$ (a) was quenched at $t^* = t(\varepsilon_1/m\sigma_1^2)^{1/2} = 0$ to a temperature $kT/\varepsilon_1 = 0.70$, producing the profile shown in b. This profile is an average over $t^* = 50$ to $t^* = 100$. The final equilibrium profile (c) is an average from $t^* = 250$ to $t^* = 550$. Argon is represented by a solid line, while krypton is represented by a dotted line.

similar and thus the mole fraction profile remains similar to that at $t^* = 0$, i.e., it is essentially uniform along the pore axis. With further equilibration, material equilibrium is established as shown in Fig. 1c. During the temperature quench mechanical equilibrium is rapidly established. Immediately after the change in temperature the system finds itself in a mechanically unstable state. Therefore small density fluctuations will grow unbounded driving the initial stages of phase separation. In contrast, material equilibrium occurs on a much slower time scale. Its relaxation time is governed by the mutual diffusion process. That is, both components must diffuse through the fluid to establish a gas phase which is richer in the more volatile component, argon. One can also see from this axial density profile that argon is positively adsorbed on the liquid–vapor interface, as expected for the more volatile component. We find argon mole fractions of $y_1 = 0.87$ and $x_1 = 0.46$ in the gas and liquid regions, respectively. The chemical potentials μ_i can be used in an additional grand canonical Monte Carlo simulation to determine the composition and pressure of the reservoir with which the pore is in equilibrium. Thus, for the composition of the gas mixture in the reservoir we find for the mole fraction of argon $x_1 = 0.77$. We refer the reader to an earlier publication [7] for phase diagrams and a detailed comparison with both the local and the nonlocal mean field DFT calculations.

It can be argued that, strictly speaking, there is no truly sharp phase transition in cylindrical geometry. Rather, as Privman and Fisher [18] have pointed out, the phase transition is expected to be rounded on a scale that is set by the cross-sectional area of the cylinder. Since the interfacial contribution is finite in cylindrical geometry, Privman and Fisher [18] argued that in a canonical ensemble multiple domains of liquid and vapor will coexist rather than single domains of each phase. In the temperature quench discussed above (see Fig. 1) we do not observe multiple domains due to the relatively low length-to-diameter ratio. However, one might expect to see multiple domains for much larger ratios. To investigate this possibility, we have performed a quench from a supercritical temperature $kT/\varepsilon_1 = 1.35$ to $kT/\varepsilon_1 = 0.60$ for a *pure* fluid confined in a pore of radius $R/\sigma_1 = 2.5$ and length $L/\sigma_1 = 720$. The axial density profile for this quench is shown in Fig. 2. After an equilibration of 100,000 Δt and accumulating averages for another 10,000 Δt, we find that the system shows 10 different regions of coexisting liquid and vapor. Note that the smallest region of liquid, which is centered around $z/\sigma_1 = 145$, still has a thickness of $\approx 8\sigma_1$. Similarly, the smallest region of gas (centered around $z/\sigma_1 = 704$), is $\approx 18\sigma_1$ thick. Both these thicknesses are significantly larger than the interfacial thickness itself, which is $\approx 3\sigma_1$. We stress, however, that one should still be cautious in interpreting these results, due to the very long equilibration
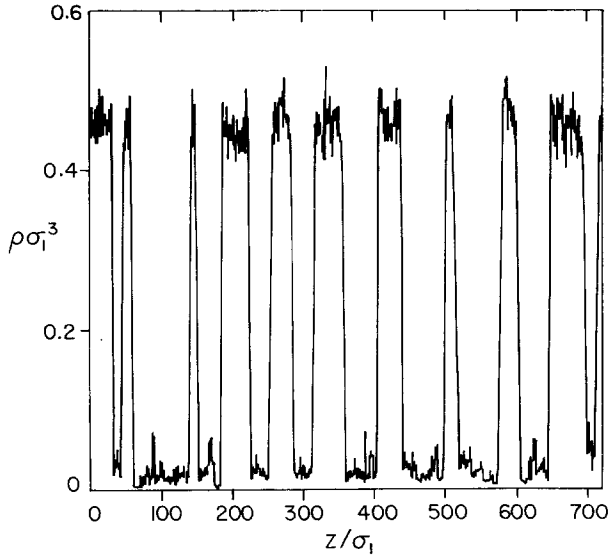
Fig. 2. Axial density profiles $\rho(z)$ for a *pure* Lennard–Jones fluid in a cylindrical pore of radius $R = 2.5\sigma_1$ and length $L/\sigma_1 = 720$. After a temperature quench from a supercritical temperature, $kT/\varepsilon_1 = 1.35$, to a temperature of $kT/\varepsilon_1 = 0.60$, the fluid phase separated, establishing multiple regions of liquid–gas coexistence.

times that might be necessary to reach a state with possibly a smaller number of domains. One way to explore this question might be to approach the problem from the opposite direction, using an initial configuration of a very long pore with only two single domains present. In addition, it would be interesting to repeat the study for a slit-like pore for which one expects only single domains due to the quasi two-dimensional geometry. Coexisting phases will also be produced when a pore is compressed, starting from a single gas-phase state. Phase separation will then be delayed, i.e., showing absorption hysteresis, and separation eventually takes place at the end of the pore-filling branch when the adsorbed fluid layer becomes unstable with respect to the formation of a biconcave lens [6]. Again, for a very long pore like the one studied here, we would expect to observe the formation of multiple lenses.

4.2. Hard Spheres Against a Hard Wall

To test the results of the DFT for arbitrary binary mixtures, we performed MC simulations for mixtures of hard spheres of different size ratios d_2/d_1. In Fig. 3 we present typical results for a mixture of size ratio of 1.5.
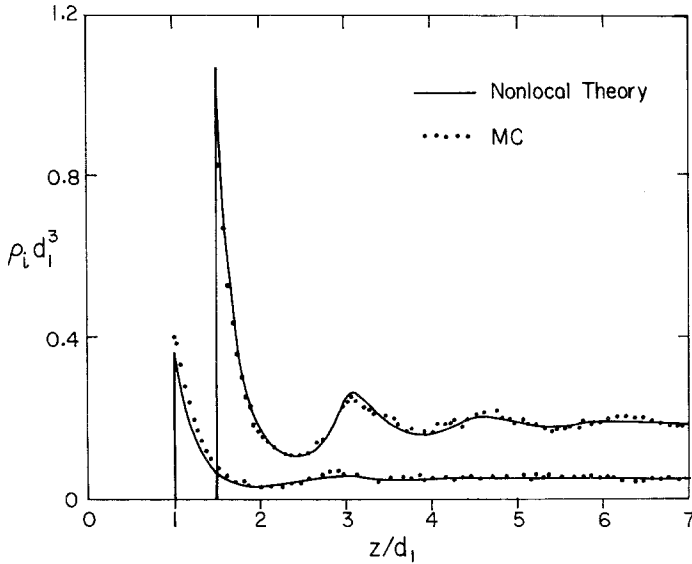
Fig. 3. Density profiles $\rho_i(z)$ for a binary hard-sphere mixture of size ratio $d_2/d_1 = 1.5$ against a hard wall. The mole fraction of species 1 is approximately 0.25. The solid lines represent the density functional theory prediction, while the dotted lines correspond to the MC results. The simulation profile has been averaged over both walls.

In the calculations we used aq total of $N = 216$ spheres, 54 of which belong to species 1. The distance between the two hard walls was $L/d_1 = 14$, which is sufficiently far apart for the profile to approximate a fluid in the presence of a *single* wall. That is, the density profiles $\rho_i(z)$ both show a non-oscillatory region in the center of the box, indicating that there is no significant interference between the walls. This allows us to average the profiles over both walls. The bulk density of each species was read from the profile, and these were used to obtain the bulk mole fraction ($x_1 \approx 0.25$) and, hence, the chemical potentials μ_i via the PY-compressibility equation of state. This information then served as input for the density functional theory [cf. Eq. (5)]. We thus force the density profiles for the theory and simulations to be the same well away from the wall. The prediction from the theory is shown as solid lines. The overall agreement is satisfying. The theory closely reproduces the oscillations of both species, and the level of agreement is similar to that found by Tarazona [9] for the pure system. However, since we truncate the weighting function expansion at first order, we must expect the agreement to be less satisfactory at higher densities and/or larger size ratios. A more detailed comparison and a full discussion of the DFT will be published shortly [10].

ACKNOWLEDGMENTS

REFERENCES

1. S.-H. Suh and J. M. D. MacElroy, *Mol. Phys.* **58**:445 (1986).
2. M. Schoen, J. H. Cushman, D. J. Diestler, and C. L. Rhykerd, Jr., *J. Chem. Phys.* **88**:1394 (1988).
3. R. Evans, U. Marini Bettolo Marconi, and P. Tarazona, *J. Chem. Phys.* **84**:2376 (1986).
4. B. K. Peterson, K. E. Gubbins, G. S. Heffelfinger, U. Marini Bettolo Marconi, and F. van Swol, *J. Chem. Phys.* **88**:6487 (1988), and references therein.
5. P. C. Ball and R. Evans, *Mol. Phys.* **63**:159 (1988).
6. G. S. Heffelfinger, F. van Swol, and K. E. Gubbins, *J. Chem. Phys.* **89**:5202 (1988).
7. G. S. Heffelfinger, Z. Tan, K. E. Gubbins, U. Marini Bettolo Marconi, and F. van Swol, *Mol. Simul.* (in press) (1988), and references therein.
8. U. Marini Bettolo Marconi and F. van Swol, Submitted for publication.
9. P. Tarazona, *Phys. Rev. A* **31**:2672 (1985).
10. Z. Tan, U. Marini Bettolo Marconi, F. van Swol, and K. E. Gubbins, *J. Chem. Phys.* (in press) (1989).
11. G. S. Heffelfinger, F. van Swol, and K. E. Gubbins, *Mol. Phys.* **61**:1381 (1987).
12. D. Brown and J. H. R. Clarke, *Mol. Phys.* **512**:1243 (1984).
13. Z. Tan, F. van Swol, and K. E. Gubbins, *Mol. Phys.* **62**:1213 (1987).
14. B. Widom, *J. Chem. Phys.* **39**:2808 (1963).
15. J. S. Rowlinson, and B. Widom, *Molecular Theory of Capillarity* (Oxford University Press, New York, 1982).
16. G. Jackson, J. S. Rowlinson, and F. van Swol, *J. Phys. Chem.* **91**:4907 (1987).
17. P. Tarazona, *Phys. Rev. A* **61**:1381 (1987).
18. V. Privman and M. E. Fisher, *J. Stat. Phys.* **33**:385 (1983); *J. Appl. Phys.* **57**:3327 (1985).